Multibaseline ATI-SAR for Robust Ocean Surface Velocity Estimation

F. LOMBARDINI, Senior Member, IEEE
F. BORDONI
F. GINI, Senior Member, IEEE
L. VERRAZZANI
University of Pisa
Italy

An open problem of along-track interferometry (ATI) for synthetic aperture radar (SAR) sensing of ocean surface currents is the need of ancillary wind information for inversion of Doppler centroid measurements, that have to be compensated for the propagation velocity of advancing and/or receding Bragg scatterers. We propose three classes of estimators which exploit multibaseline (MB) ATI acquisition and Doppler resolution for robust data inversion under different degrees of *a priori* information about the wind direction and the value of the characteristic Bragg frequency. Performance analysis and comparison with conventional ATI show that the proposed MB estimators can produce accurate velocity estimates in the absence of detailed ancillary data.

Manuscript received August 26, 2002; revised August 20 and December 22, 2003; released for publication December 22, 2003.

IEEE Log No. T-AES/40/2/831349.

Refereeing of this contribution was handled by E. S. Chornoboy.

This work has been supported by the Italian National Research Council (CNR-IENT).

Authors' address: Dept. of "Ingegneria dell'Informazione," University of Pisa, via Caruso, I-56122, Pisa, Italy, E-mail: (lombardini@iet.unipi.it).

0018-9251/04/$17.00 © 2004 IEEE

I. INTRODUCTION

Along-track synthetic aperture radar interferometry (ATI-SAR) for ocean surface velocity sensing is a relatively new technique for remote sensing introduced in 1987 by NASA-JPL researchers [1]. It is currently recognized that ATI-SAR is a very promising tool for microwave active ocean sensing, with the same night-and-day, all-weather operational capability of SAR, but capable of producing much richer information. However, theory and experiments of interferometric ocean sensing are still evolving and the technique is not in a mature operational status, yet. To contribute to its spreading, a special session on interferometric applications over the ocean has been organized in the 2001 IEEE International Geoscience and Remote Sensing Symposium; a specific session has been also dedicated to ATI-SAR within the 2002 NASA AIRSAR Earth Science and Application Workshop [2]. The basic concepts of ATI are recalled in what follows.

The original ATI technique uses a two-antenna SAR system, as shown in Fig. 1. Despite Doppler

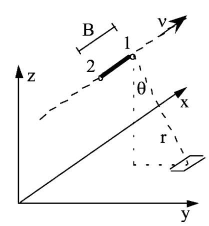

Fig. 1. Configuration of ATI-SAR acquisition (x, flight axis; y, ground range; z, altitude; B, baseline between the two-way phase centers; v, platform speed; θ, off-nadir angle; r, slant range distance).

information being virtually lost during SAR processing, Doppler shifts can be detected if the signal is acquired and processed a second time. The along-track baseline between the two elements of the interferometer produces the required short time lag τ between the two complex SAR images formed by the returns received at each antenna. These are focused through proper motion compensation and coregistered [3–4]. Estimation of the interferometric phase difference φ between the two images allows us to measure the mean short-term Doppler shift $\bar{\omega}$ of the scattering from the ocean surface on a pixel-by-pixel basis, through the relationship $\varphi = \bar{\omega}\tau$ [5]. To get absolute Doppler measurements, the interferometric phase has first to be calibrated. This can be carried out by exploiting a patch of terrain in the imaged scene, for which $\bar{\omega} = 0$. If land is not imaged together with the ocean, one can exploit for calibration velocity measurements of ships in the scene, obtained through the azimuth misplacement effect between the ship and its wake in the SAR image [6]. After obtaining the Doppler measurements, one has to compensate for the net velocity of the short radar-wavelength resonant wind waves, i.e. the Bragg waves that are responsible of the scattering itself [7–8]. This results in the radial (slant-range) surface velocity. It can be converted to a ground-range velocity by projection according to the off-nadir illumination angle [3]. The measured surface velocity is composed of translational motions and long (resolved) wave orbital motions [7, 5]. Therefore, ATI systems have the potential to directly measure ocean surface currents, tidal currents, and other surface dynamical features, at large scale and with high spatial resolution [1, 5, 9, 3]. Additionally, directional sea wavenumber spectra can be derived from the ATI phase map by two-dimensional Fourier transform [1]. In fact, long wave orbital motions directly produce signatures in the phase map, and line-of-sight velocities are related to height of the ocean waves via linear wave theory. The ATI wavenumber spectra exhibit higher azimuth wavenumber bandwidth and linearity than inversion methods based on single SAR amplitude image [10–11]. When a full velocity field has to be measured, instead of only the ground-range component, successive measurements from crossed flight paths can be integrated, or vector-ATI systems may be used which are being envisaged for simultaneous ATI acquisition with different squint angles [12–13]. The coherence time of the backscattered radar signal is also measurable by ATI through the correlation coefficient between the two complex SAR images [3]. It provides information on subresolution scale processes of the ocean surface. In fact, the scatterer ensemble coherence time is mainly determined by modulation of the velocity of Bragg waves from medium (non-resolved) waves, which results in a distribution of slant-range velocities in the given SAR resolution cell [7].

Concerning ATI system design, the most important parameter is the time lag τ, which is chosen as a trade-off among interferometer sensitivity, signal decorrelation, Doppler unambiguous estimation range, and azimuth wavenumber bandwidth in the retrieval of sea wave spectra [3, 10]. In particular, for a given coherence time, an increase of the time lag produces higher velocity sensitivity of the along-track interferometer, but this is obtained at the cost of increased decorrelation and so larger phase noise. How the resulting velocity estimation accuracy is affected by the time lag depends on the trade-off between the two effects, that is particularly important when the signal to noise ratio or the number of looks in the SAR images are low [3]. A more extended description of the basics of ATI can be found in [8], [14], and [4].

The existing and potential applications of these ATI capabilities are various: scientific, environmental, and commercial. ATI can provide rich information about surface currents and waves, internal waves, eddies, shears, upwelling processes [8], which are of considerable interest in oceanographic investigations, hydrology, meteorological forecasts, environmental management, coastal protection, fishery, off-shore industry, and ship transportation. In order to exploit its potentiality, the basic technique of ATI has been recently evolved in the direction of multibaseline (MB) ATI, that employs more than two phase centers displaced along-the-track [3, 15–17]. A brief overview of the research on advanced MB-ATI processing to reduce data noise and blurring that can affect conventional ATI can be found in [18].

A basic problem of ATI sensing concerns the extraction of maps of physical parameters from the maps of estimated radar parameters. In particular, for reliable inversion of surface velocities from Doppler maps, accurate ancillary data of local surface wind direction (and possibly speed) are necessary to evaluate a reference spectrum of speckle, determined by Bragg waves [5]. In fact, surface velocity from translational and orbital motions is proportional to the shift (advection) of the speckle spectrum from the zero-velocity (ambient) situation.[1] Alternatively, for coastal applications one might resort to a zero-current reference Doppler centroid, obtained by extending the flight path over a reservoir of standing water with similar wind conditions [9]. However, this is a very particular situation. In both cases, velocities are estimated from the shift of the estimated Doppler centroid with respect to that of the reference spectrum [19]. In general, the reference spectrum can be bimodal when both advancing and receding Bragg waves are present in the resolution cell, for a geometry different from up or downwind.[2] This is due to the directional spread of wind-generated Bragg waves, and the power distribution between the two possible Bragg components depends on the wind aspect. This is often not well known and highly varying over the scene. Conventional ATI is "blind" to the spectrum shape and can only measure the Doppler centroid. Therefore, it produces highly biased estimates of surface velocities if the local wind direction is not a-priori known and accurate compensation for the phase velocities of the Bragg wave components is not possible [5, 20, 19, 21]. In fact, an unexpected power split ratio between the two Bragg components results in an unmodeled shift of the Doppler centroid (see Fig. 2). This prevents ATI-SAR from being a flexible, reliable, and fully automatic remote sensing technique.[3]

[1]Advection is a radar-oceanography jargon referring to the translational motion superimposed by a current flow or by the instantaneous value of a wave orbital velocity to the propagation velocity of a smaller wavelength wave in the steady medium (see e.g. [5, p. 10,262]. In this paper, we use the same term also for the corresponding spectral shift of the spectrum of the backscattered signal, caused by the superimposed translational motion.

[2]The jargon for this dual Bragg component condition, when the components are resolved, is "Bragg splitting."

[3]It is worth noting that the presence of a dual Bragg component can also affect the variance of the surface velocity estimate, which

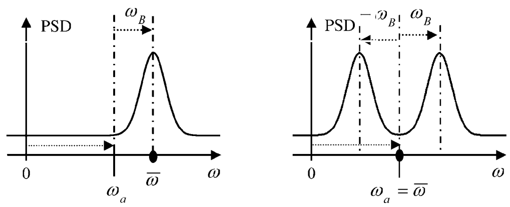

Fig. 2. Bragg uncertainty issue. (left) Short-term Doppler spectrum for upwind, advection from surface velocity ω_a, characteristic Bragg frequency from Bragg propagation velocity ω_B, Doppler centroid $\bar{\omega}$. (right) Crosswind, note different offset between Doppler centroid and spectrum advection.

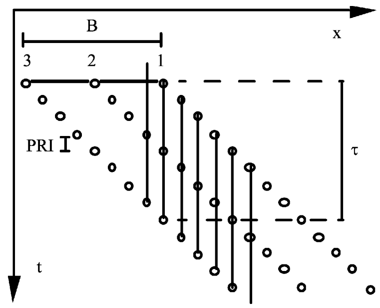

Fig. 3. Dual baseline ATI-SAR (K = 3).

This paper addresses the possibility of exploiting MB acquisition in a new way, to cope with the Bragg uncertainty issue. Exploitation of MB-ATI data is investigated to produce estimate of ocean surface velocity that is autonomous from detailed in-situ ancillary information and intrinsically robust to possible bimodal spectrum scenarios, as originally hinted in [5]. The goal here is to develop this concept relying on the advanced MB functionality of resolution in the Doppler shift domain [15–17], and resorting to high- or superresolution spectral analysis and proper "locking" onto the estimated Bragg peaks.

The rest of this paper is organized as follows. An MB statistical data model is presented in Section II, based on classical assumptions of radar oceanography. The spectral advection estimation problem under uncertain Bragg situation is also stated. In Section III, a robust advection estimation technique is proposed which is based on a two-step procedure. For both steps, different solutions are proposed and analyzed. For MB ATI Doppler analysis, we investigate the application of the multilook periodogram and of the adaptive Capon filter. Superresolution autoregressive (AR) and combined multiple signal classification (MUSIC)-least squares (LS) spectral estimation is also considered. Then, different locking methods are proposed coupled with the above mentioned spectral estimators, producing three different classes of MB robust velocity estimators, which exploit different degrees of a priori information about the wind direction and the value of the characteristic Bragg frequency. In Section IV, the accuracy of the proposed MB robust estimators is investigated through Monte Carlo simulation and Cramér-Rao lower bound (CRLB) analysis, and compared with conventional ATI. Some concluding remarks can be found in Section V. The derivation of the CRLB for MB advection estimation is outlined in the Appendix.

can be higher than in the single Bragg component condition. This is because the mixing of the two Bragg components lowers the overall coherence time, for a same modulation effect from medium waves [18]. Higher variance negatively affects also the wavenumber spectra estimate, whose noise floor is raised.

II. DATA MODEL AND PROBLEM STATEMENT

Consider MB-ATI data from a uniform linear array of K two-way phase centers with overall baseline B, onboard a platform moving at speed v. This along-track array can be obtained by using K antennas with an overall baseline $2B$, with one transmit/receive antenna and the other antennas only used on reception (see [1, 22–23] for K = 2, 3, and 4, respectively). Alternatively, for K = 3 one can resort to transmitter "ping-ponging" between just two antennas with a baseline B, effectively synthesizing three different equispaced two-way phase centers [3]. The MB along-track array acquires K complex SAR images at $K-1$ time lags $\{l\tau/(K-1)\}_{l=1}^{K-1}$, where $\tau = B/v$ is the overall time lag. As an example, Fig. 3 shows the space-time location of the phase centers for K = 3; x is the flight axis and PRI is the SAR pulse repetition interval. Note that although the PRI is an integer submultiple of τ in Fig. 3, this condition is not necessary, image alignment can be performed in the coregistration stage [23]. From the three synthetic apertures, three SAR images of the same area can be obtained in identical geometry and with time lags $\tau/2$ and τ. The complex amplitudes of the pixels corresponding to a same given patch of sea can be arranged to form the $K \times 1$ vector $\mathbf{y}(n) = [y_1(n) \cdots y_K(n)]^T$, for $n = 1,2,\ldots,N$, where N is the number of available independent and identically distributed looks [3].

The statistical model of the MB SAR-processed echoes adopted here is based on the classical two-scale electromagnetic model of ocean backscattering [7]. Accordingly, each data vector is modeled as [24]:

$$\mathbf{y}(n) = \sigma_1 \mathbf{A}(\omega_1\tau)\mathbf{x}_1(n) + \sigma_2 \mathbf{A}(\omega_2\tau)\mathbf{x}_2(n) + \mathbf{v}(n) \quad (1)$$

where $\mathbf{A}(\omega\tau)$ is the $K \times K$ diagonal matrix having on the main diagonal the elements of the steering vector $\mathbf{a}(\omega\tau) = [1 \;\; e^{j\omega\tau/(K-1)} \cdots e^{j\omega\tau}]^T$; ω_i is the Doppler shift of the backscattered signal from the advancing (i = 1) or receding (i = 2) Bragg component considered in isolation, and σ_i^2 is the corresponding mean power. Note that taking account of the typical small τ values (5–100 ms [3]), the large scale variation of ocean structure can be neglected in the temporal multichannel model (1). This corresponds to treat deterministically orbital velocities of long waves [19, p. 450], and this is why the powers σ_i^2 and the short-term Doppler shifts ω_i are assumed to be constant over the ATI observation interval τ. The two cisoids corresponding to the Bragg components are corrupted by complex multiplicative noise arising from modulation by medium waves. The multiplicative noise is modeled by the $K \times 1$ complex vectors $\{\mathbf{x}_i(n)\}$; it takes into account the random phase and amplitude changes of the backscattered signal during the ATI observation interval. In the radar imaging jargon, $\mathbf{x}_i(n)$ is the speckle term for the nth look, for the ith Bragg component in isolation. It is modeled as a circular Gaussian distributed random vector. Considering freely-propagating Bragg waves, which are typical for L- and C-band systems, the autocorrelation sequence of each speckle component can be assumed to be real and Gaussian-shaped for light to gentle wind and large to moderate off-nadir incidence angle [5, 19]. Therefore, the elements of the covariance matrix of $\{\mathbf{x}_i(n);\ i = 1,2\}$ are given by

$$\begin{aligned}[\mathbf{C}_x]_{l,m} &= [E\{\mathbf{x}_i(n)\mathbf{x}_i^H(n)\}]_{l,m} \\ &= \exp\{-[(l-m)\tau/(K-1)\tau_c]^2\}, \\ &\qquad l,m = 1,2,\ldots,K, \qquad \forall \quad n \end{aligned} \tag{2}$$

where $(\cdot)^H$ denotes conjugate transpose and τ_c is the coherence time. In what follows we refer to $\tilde{\tau}_c = \tau_c/\tau$ as the normalized coherence time. Note that here we refer to the coherence time of each Bragg component considered in isolation, not to the conventional overall ocean coherence time. Under the above-mentioned assumptions, the contribution of ith Bragg source to the power spectral density (PSD) is Gaussian-shaped and centred on ω_i.[4] The spectral Gaussianity is a well-known result arising through the Central Limit Theorem from the large number of modulating medium waves, which locally advect the Bragg waves in the resolution cell by their orbital motion [19]. Generally speaking, an offset δ_{ω_B} may arise between the centroid of the Bragg spectral component and the frequency ω_i of the unperturbed Bragg component. This is due to the so-called tilt modulation effect, which produces correlation between amplitude and frequency modulation of the backscattered signal [5, 25]. In fact, both reflectivity and instantaneous velocity are functions of the position along the modulating wave phase, through the local surface tilt and orbital motion, respectively. However, as it is discussed after completing the description of the model, the tilt modulation effect from medium waves in ATI is negligible under our system band, incidence angle, and wind speed assumptions; this is why the Bragg spectral components in our model are centred on ω_i. The $K \times 1$ complex vector $\mathbf{v}(n)$ in (1) models the thermal noise, which is additive white Gaussian with power σ_v^2. Vectors $\mathbf{x}_1(n)$ and $\mathbf{x}_2(n)$ are assumed to be independent, because they model the backscattered echoes from different sources, and independent of $\mathbf{v}(n)$. The Doppler frequencies of the two Bragg components are related to spectrum advection ω_a by

$$\omega_1 = \omega_a + \omega_B, \qquad \omega_2 = \omega_a - \omega_B \tag{3}$$

where ω_B is the Bragg frequency [5, 19]. Given the radar operative parameters carrier wavelength λ and off-nadir angle ϑ, the wavelength of the Bragg waves is determined by the condition of constructive interference to the radar sensor. Under the free-propagation assumption, their own consequent propagation velocity is determined by the dispersion relation of the medium. As an example, for L- and C-band systems, where the Bragg waves are gravity waves, the corresponding characteristic Bragg frequency is $\omega_B = \sqrt{4\pi g \sin(\vartheta)/\lambda}$, where $g = 9.81\ \mathrm{ms}^{-2}$ is the constant of gravity acceleration [21].

Some remarks on the tilt modulation effect are now in order. Tilt modulation is a radar-oceanography jargon used in the context of the coupling of radar reflectivity variations along the profile of a modulating wave with variations of the instantaneous modulation velocity. The coupling arises because both reflectivity and velocity are functions of the position along the modulating wave phase. The modulation velocities associated with stronger reflectivities have larger weight in the spectrum over the others. As a result, the Bragg Gaussian spectral component can be offset from the theoretical frequency of the unperturbed Bragg line component, an expression for this offset is represented by the integral in [19, eq. (10)], $\delta_{\omega_B} = \mathrm{Re}\left\{\iint D^*(\mathbf{k})M_{1\pm}(\mathbf{k})k^2\Psi(\mathbf{k})d^2k\right\}$, where $(\cdot)^*$ denotes conjugate. It depends on the so-called Doppler modulation transfer function (MTF) $D(\mathbf{k})$, the directional wavenumber spectrum $\Psi(\mathbf{k})$, and the (amplitude) MTFs $M_{1\pm}(\mathbf{k})$ for the advancing and receding Bragg waves, respectively, where $\mathbf{k}$ is the wavenumber of the generic modulating wave, and $k = |\mathbf{k}|$ [19]. The Doppler MTF is used to express the instantaneous Doppler variations which are linear in the surface slope. It depends on the carrier wavelength, off-nadir angle, and wind aspect. The amplitude MTFs describe the oscillations of the mean signal intensity which are linear in the slope variations of the modulating wave and hence in the variation of the Doppler frequency. The two amplitude MTFs $M_{1+}(\mathbf{k})$ and $M_{1-}(\mathbf{k})$ can be considered to be equal neglecting the effect of the so-called hydrodynamic interaction, which varies the Bragg wave intensity along longer waves, yet

[4] As in [5, 3, 16], this model does not take into account possible azimuth blurring from velocity bunching [9, 19]. This may be reduced by MB methods, as well [15, 16, 18]. For the meaning, scope and limitations of this modeling framework see also [16].

producing only small deviations from simpler models [19, p. 451–452]. Thus, the possible offset from the theoretical Bragg frequency can be assumed to be equal for the advancing and the receding Bragg component. This Doppler offset can be observed in some plots reporting numerical and experimental data in [5, 25, 19] (in [25], Doppler information can be derived from the interferometric phase information in the plots thanks to the relationship $\omega = \varphi/\tau$). The offset tends to increase with wind speed and carrier frequency, and for decreasing off-nadir angle and wind aspect approaching upwind or downwind [5, p. 10,261–10,262]. In certain critical situations, tilt modulation can also make the Bragg spectral component become skewed non-Gaussian, see [5, top right plot in Fig. 1] (10 m/s wind speed-fresh wind, C-band, 20 deg off-nadir angle-steep incidence, downwind).

However, this Doppler offset and possible skewness are produced by tilt modulation when observation time is long and/or the backscattering ocean patch is large compared with the dominant wave period or length, respectively.[5] Conversely, our ATI model has to account for the statistics of the backscattered signal from a finite little ocean patch over a short time window. The patch size is given by the area of the SAR pixels, possibly accounting for defocusing typical in ocean imaging [3] (see again footnote 4). As observation interval we can assume the time lag τ, whose order of magnitude is 100 ms in L-band and 10 ms in C-band [3]. Thus, model (1)–(3) has to account for the short-term Doppler spectrum from a limited area, not for the long-term and/or spatially averaged Doppler spectrum in [5, 19]. In our framework, the long waves are treated deterministically, as already noted in the beginning of this section, and their instantaneous orbital velocity becomes part of the measured surface velocity. Thus, the possible significant tilt modulation effect by long waves does not affect the signal in the ATI framework.

In this sense, we can use the results in [19] and [5] to draw a few conservative limits to our statistical model. It is in very good agreement with the physical model in [19, eqs. (10)–(13)] for low wind speed, when the tilt modulation effect is surely negligible even when long waves are accounted for, at least for wind aspect close to crosswind [5, p. 10,262]. See, e.g., [19, top plot in Fig. 1] (3 m/s-light wind, L-band, 30 deg off-nadir angle, wind aspect 15 deg away from crosswind) and [5, bottom left plot of Fig. 1] (crosswind, the other parameters similar to the above-mentioned). From these examples, where the spectral peaks are centered at the frequencies ω_i of the unperturbed Bragg components, we can draw a sample condition of wind speed, carrier frequency, off-nadir angle, and wind aspect range for which our model surely matches the expected behavior from Bragg scattering-based composite surface models [19] and Maxwell-based fundamental backscattering models [5]. Noteworthy, these limits for the validity of our ATI model are conservative, since only tilt modulation from the medium waves could actually produce a Doppler offset not accounted for in (1)–(3). Detailed evaluation of the effective limits for our model would require computation of the Doppler offset integral equation in [19, eq. (10)] for the pertinent wavenumber spectrum, integrating just down to a minimum wavenumber dictated by the SAR resolution cell, thus excluding longer waves than the medium waves. In this framework, a relaxed more useful sample condition of wind speed, carrier frequency, and wind aspect range for which our model is still a good approximation of the real short-term spectrum can be drawn from some results in [25]. Analyses of data in Ka-band (35 GHz) are reported there, from a limited ocean patch (scatterometer footprint dimension significantly smaller than that of the dominant long wave), with off-nadir angle 45 deg, almost upwind wind aspect, and wind speed around 5 m/s (gentle wind). The corresponding short-term spectra in [25, Fig. 4], computed with a 250 ms time window, do not show any sensible skewness effect. Still, this does not rule out a possible offset of the Gaussian-shaped short-term Doppler spectrum with respect to the theoretical Bragg frequency. Yet, indications can be derived from [25, Fig. 9] that the possible offset due to the light tilt modulation effect from medium waves is negligible, indeed. There, estimators of the centroid of the short-term Doppler spectrum, which are sensitive to possible offset due to tilt modulation, are compared with the estimated mean of the instantaneous frequency which is not affected by possible tilt modulation. The comparison, for the 250 ms time window, shows that the offset in the short-term spectrum must be negligible (see at p. 16,300). Thus, our model (1)–(3) is still a very good approximation of reality also for Ka-band, 5 m/s wind speed, upwind. Consider now that offset from tilt modulation in the long-term spectrum is less sensible for lower carrier frequencies (e.g. L-band) than for Ka-band [25, p. 16,295]. Therefore, it is reasonable that the possible offset in the short-term spectrum, which is negligible in Ka-band, is negligible also for typical bands employed in ATI and on which our paper is focused (L- and C-band), for the same 5 m/s wind speed.

Summarizing, from the above-mentioned trends and examples we can infer that our model, in which

[5]The backscattering patch size assumed for numerical evaluation in [19] is infinite (see at p. 450 and p. 456), and the Doppler spectrum is averaged over all the long-wave phase locations for numerical evaluation in [5] (see at p. 10,262). The Doppler spectrum is averaged over a 5 min time window for measurements in [25] (see at p. 16,295–16,296).

spectral offsets from tilt modulation are assumed to be negligible, is valid at L- and C-band for ATI multilook patch smaller than the dominant wave length, light to gentle wind, any wind aspect, and large to moderate off-nadir angles greater than or equal to 45 deg (note that these limits may still be conservative). Of course, some offset might arise even in the short-term spectrum in extreme wind conditions, steeper incidence or higher carrier frequencies, but this can be quantified by proper computation of integral [19, eq. (10)] for the specific situation at hand, and is left as matter for future research. When one trespasses these effective limits, the unmodeled offset results in a bias to be added to the residual bias of the robust velocity estimators, designed for robustness to unknown power split ratio only, which is analyzed in Section IV. However, note that when wind speed increases system operation may be impaired simply by large estimation variance from low coherence time, before the unmodeled bias becomes a real problem.

The velocity inversion problem considered here can be cast as the problem of estimating the spectral advection ω_a from MB data $\{\mathbf{y}(n)\}_{n=1}^{N}$, with unknown deterministic nuisance parameters: the power split ratio (or differential signal-to-noise ratio) $\Delta\mathrm{SNR} = \sigma_1^2/\sigma_2^2$; the total signal power $\sigma_T^2 = \sigma_1^2 + \sigma_2^2$; the coherence time of the multiplicative noise τ_c; the thermal noise power σ_v^2. The lack of detailed knowledge of ΔSNR is the most troublesome for the inversion problem. As discussed in Section III, in some circumstances also the characteristic Bragg frequency ω_B should be modeled as an unknown deterministic parameter.

III. ROBUST VELOCITY ESTIMATION

The general approach to the estimation of unknown deterministic parameters is the maximum likelihood (ML) method, because of its desirable statistical properties [26, ch. 7]. ML estimation could be applied to our problem to estimate ω_a. This would require maximization of the nonconvex likelihood function with respect to all the unknown parameters, leading to a too high computational burden [16]. Hence, ML estimation of ω_a is not feasible in practical applications and has to be abandoned for computationally simpler alternatives.

In the work presented here we solve the estimation problem by means of a two-step procedure. The two steps can be termed: 1) MB Doppler analysis, and 2) locking. In step 1, we resolve the two spectral peaks of the bimodal spectrum. In MB systems, the availability of a signal temporal history, $K > 2$ time samples, offers to ATI the advanced functionality of resolution in the Doppler frequency domain. This has been proposed in [15] and [17] for deblurring the intensity image and for clutter filtering, respectively. Here, we exploit the Doppler resolution capability in a different way. After proper Doppler analysis of the MB data, in step 2 we retrieve unambiguously ω_a, using the locations of Bragg peaks as stable markers of the advection. In fact, the offset between the Bragg peak locations (3) and the value of ω_a is independent of the unknown power split ratio ΔSNR, differently from what happens for the conventionally used Doppler centroid. Step 2 is composed of a "labeling" stage, in which the two frequency estimates are associated to the advancing and receding Bragg components, and a "locking" onto the Bragg peaks stage. Locking the advection estimate onto the Bragg peaks is possible assuming that the ambient spectrum peaks at the frequency of the advancing and receding free Bragg components. This condition is valid for light to gentle wind, large to moderate incidence angle, and low carrier frequency (L-, C-band), as discussed above. Proper MB spectrum resolution and identification by the proposed two-step procedure should result in a surface velocity estimate that is not heavily hampered by a change of the signal power split ratio between the two Bragg components.

A. MB Doppler Analysis

The MB spectral estimation task is challenging because of the typically short time span τ of the data, that can result in insufficient resolution. Also, spectral leakage can mask a Bragg component when weak. For this reason different spectral estimation methods, either nonparametric or parametric, have been applied to the ATI problem at hand and compared. The Doppler analysis step has to provide two pieces of information that will be used in the second step of the procedure: a) an estimate of the location of the Bragg peaks, and b) the indication of which one of the two peaks is the strongest.

The multilook version of the classical nonparametric periodogram method, beamforming, can be applied to this aim. Beamforming filters the N data vectors with a complex finite impulse response (FIR) filter of length K designed to pass undistorted the signal component at frequency ω and minimize the output interfering power from all the other frequencies, assuming a white spectrum [27]. The spectrum estimate, neglecting a scaling factor unnecessary in our application, is obtained from the estimated mean output power and is given by

$$\hat{P}_{\mathrm{BF}}(\omega) = \mathbf{a}^H(\omega\tau)\hat{\mathbf{C}}_y\mathbf{a}(\omega\tau)/K^2 \qquad (4)$$

where $\hat{\mathbf{C}}_y$ is an estimate of the data covariance matrix. When $\hat{\mathbf{C}}_y$ is the sample covariance matrix, estimator (4) coincides with the periodogram of the data vector $\mathbf{y}(n)$ averaged over the N looks [27]. Therefore, the resolution properties of beamforming are analogous to those of the periodogram method. This sets the conventional Fourier resolution limit at

$\Delta\omega_{\mathrm{BF}} = 2\pi(K-1)/(K\tau)$. The "unlabeled" frequency estimates $\hat{\omega}_{\mathrm{I}}$ and $\hat{\omega}_{\mathrm{II}}$ of the two Bragg components are derived as the locations of the two highest peaks of $\hat{P}_{\mathrm{BF}}(\omega)$. The corresponding powers σ_{I}^2 and σ_{II}^2 of the two components are estimated as the values of $\hat{P}_{\mathrm{BF}}(\omega)$ at these locations. The estimates $\hat{\omega}_{\mathrm{I}}$, $\hat{\omega}_{\mathrm{II}}$ will be associated in step 2 to the frequencies ω_1 and ω_2 of the advancing and receding components. It is worth noting that in practical applications the number K of complex SAR images is usually between 3 and 5 [22, 3, 16–17, 28], and spectral estimation from a very low number K of time samples has peculiar characteristics, independently of the number N of available looks. The discrete squared-sinc-shaped spectral response of periodogram to a line component has a very low number of high sidelobes in the unambiguous Doppler range $2\pi(K-1)/\tau$. For $K = 3$, a single sidelobe is present and numerical analysis shows that when two components of similar power are unresolved, the spectral response can exhibit a unique peak with a negligible sidelobe. If the beamforming spectral estimate is unimodal, we allow for step 1 to return a flag for those locking methods of step 2 which require both Bragg components to be estimated, as will be described in the sequel.

To get better resolution than the Fourier limit and reduce leakage problems, we applied modern spectral estimators to the ATI problem as an alternative to beamforming. The first method is the high-resolution nonparametric adaptive Capon's filter. It is derived under the same condition of minimum interfering power as beamforming, but considering the general case of nonwhite spectrum [27]. The Capon power spectrum estimate is

$$\hat{P}_{\mathrm{CP}}(\omega) = [\mathbf{a}^H(\omega\tau)\hat{\mathbf{C}}_y^{-1}\mathbf{a}(\omega\tau)]^{-1}. \tag{5}$$

Estimates $\hat{\omega}_{\mathrm{I}}$, $\hat{\omega}_{\mathrm{II}}$, $\hat{\sigma}_{\mathrm{I}}^2$, and $\hat{\sigma}_{\mathrm{II}}^2$ are obtained as the locations and the amplitudes of the two highest peaks of $\hat{P}_{\mathrm{CP}}(\omega)$. A flag is returned if only one peak is found.

Beamforming and Capon methods can be used without any knowledge of the data statistical properties. On the other hand, their performance is expected to be lower than that achievable by parametric viz. superresolution methods, provided that the assumed model fits well the data. Based on this fact, we also investigate the use of the popular MUSIC frequency estimator coupled with the LS amplitude estimator. MUSIC is a parametric method for estimating sinusoidal signals embedded in additive white noise; it relies on the data covariance matrix eigendecomposition [27]. In our application, in the absence of multiplicative noise we can assume two sinusoidal components, corresponding to the two Bragg lines in the PSD. Denoting by $\{\lambda_1,\ldots,\lambda_K\}$ the eigenvalues of the data covariance matrix $\mathbf{C}_y$ arranged in nonincreasing order, these can be split into two subsets, $\{\lambda_k\}_{k=1}^2$, and $\{\lambda_k\}_{k=3}^K$, with the elements of first and second subset being greater than and equal to σ_v^2, respectively. Denote by $\{\mathbf{s}_1,\mathbf{s}_2\}$ the "signal" eigenvectors which correspond to the first two eigenvalues, and by $\{\mathbf{n}_1,\ldots,\mathbf{n}_{K-2}\}$ the "noise" eigenvectors which correspond to the remaining $K-2$ eigenvalues. Then, let $\mathbf{S} = [\mathbf{s}_1\ \ \mathbf{s}_2]$ and $\mathbf{N} = [\mathbf{n}_1 \cdots \mathbf{n}_{K-2}]$ be the matrices collecting the signal and noise eigenvectors, respectively. MUSIC exploits the property that the steering vector $\mathbf{a}(\omega\tau)$, evaluated at the frequencies ω_1 and ω_2, is orthogonal to the noise subspace spanned by $\mathbf{N}$. The polynomial version of MUSIC, root-MUSIC, is employed here [27]. It determines the two frequency estimates from the angular position of the two roots, which are located nearest the unit circle, of the polynomial

$$\mathbf{a}^T(z^{-1})\hat{\mathbf{N}}\hat{\mathbf{N}}^H\mathbf{a}(z) = 0 \tag{6}$$

where $\hat{\mathbf{N}}$ denotes the matrix comprising the noise eigenvectors derived from the eigendecomposition of the estimated covariance matrix $\hat{\mathbf{C}}_y$, and $\mathbf{a}(z) = [1\ \ z \cdots z^{(K-1)}]^T$ is the steering vector with $\exp[j\omega\tau/(K-1)]$ replaced by z. Estimates $\hat{\omega}_{\mathrm{I}}$ and $\hat{\omega}_{\mathrm{II}}$ are obtained as the angles of the roots times $(K-1)/\tau$. MUSIC does not produce a true PSD, thus it does not allow us to identify the strongest Bragg component. Therefore, we evaluate the power of the Bragg components by resorting to the LS method. This is a parametric algorithm for amplitude analysis of sinusoidal signals in additive noise. It is adopted here in its multilook version [27]. If the frequencies ω_{I} and ω_{II} were known, the amplitudes of the two sinusoidal components could be jointly estimated by minimizing the squared error between the model and the data:

$$J_N[\alpha_{\mathrm{I}}(n),\alpha_{\mathrm{II}}(n)] = \sum_{n=1}^{N} \|\mathbf{y}(n) - \alpha_{\mathrm{I}}(n)\mathbf{a}(\omega_{\mathrm{I}}\tau) - \alpha_{\mathrm{II}}(n)\mathbf{a}(\omega_{\mathrm{II}}\tau)\|^2 \tag{7}$$

with respect to $\{\alpha_{\mathrm{I}}(n),\alpha_{\mathrm{II}}(n)\}_{n=1}^N$. $\alpha_{\mathrm{I}}(n)$ and $\alpha_{\mathrm{II}}(n)$ are the two unknown complex amplitudes for the nth look, and $\|\cdot\|^2$ denotes the Euclidean norm. Minimization with respect to the complex amplitudes leads to the pseudoinverse linear solution:

$$\begin{bmatrix} \hat{\alpha}_{\mathrm{I}}(n) \\ \hat{\alpha}_{\mathrm{II}}(n) \end{bmatrix} = [(\mathbf{\Lambda}^H\mathbf{\Lambda})^{-1}\mathbf{\Lambda}^H]\mathbf{y}(n) = \begin{bmatrix} \mathbf{b}_{\mathrm{I}}^H(\omega_{\mathrm{I}},\omega_{\mathrm{II}}) \\ \mathbf{b}_{\mathrm{II}}^H(\omega_{\mathrm{I}},\omega_{\mathrm{II}}) \end{bmatrix} \mathbf{y}(n) \tag{8}$$

where $\mathbf{\Lambda} = [\mathbf{a}(\omega_{\mathrm{I}}\tau)\ \ \mathbf{a}(\omega_{\mathrm{II}}\tau)]$; $\mathbf{b}_{\mathrm{I}}^H$ and $\mathbf{b}_{\mathrm{II}}^H$ are the first and second row of the $2\times K$ matrix $(\mathbf{\Lambda}^H\mathbf{\Lambda})^{-1}\mathbf{\Lambda}^H$, respectively. In practice, matrix $\mathbf{\Lambda}$ is replaced by $\hat{\mathbf{\Lambda}} = [\mathbf{a}(\hat{\omega}_{\mathrm{I}}\tau)\ \ \mathbf{a}(\hat{\omega}_{\mathrm{II}}\tau)]$, where $\hat{\omega}_{\mathrm{I}}$ and $\hat{\omega}_{\mathrm{II}}$ are obtained using MUSIC; similarly, $\mathbf{b}_{\mathrm{I}}^H$ and $\mathbf{b}_{\mathrm{II}}^H$ are replaced by the corresponding $\hat{\mathbf{b}}_{\mathrm{I}}^H$, $\hat{\mathbf{b}}_{\mathrm{II}}^H$. Once the complex amplitude estimates are derived for each look, we can estimate the mean power of the two Bragg components as the sample variance:

$$\hat{\sigma}_l^2 = \frac{1}{N}\sum_{n=1}^{N} |\hat{\alpha}_l(n)|^2 = \hat{\mathbf{b}}_l^H \hat{\mathbf{C}}_y \hat{\mathbf{b}}_l, \qquad \text{for} \quad l = \mathrm{I}, \mathrm{II} \tag{9}$$

where $\hat{\mathbf{C}}_y$ is the sample estimated covariance matrix. Note that the method based on root-MUSIC and LS always produces two estimates of frequencies and powers, conversely from beamforming and Capon. However, this method operates under model mismatch when the speckle term affecting the Bragg components is not completely correlated, i.e., τ_c is finite. Nevertheless, it should outperform beamforming and Capon when τ_c is significantly larger than the observation time τ [29].

In the attempt to get better model matching with the nondiscrete spectrum arising from speckle decorrelation, AR spectral estimation has also been investigated. An all-pole rational spectrum model has been assumed with the order P selected in the range $[2, \ldots, K-1]$. In this work, the Yule-Walker (YW) method is employed to estimate the AR polynomial coefficients [27]. This method exploits the linear relationship between these coefficients and the autocovariance values. We obtain the AR coefficients from the solution of a nonoverdetermined YW system of equations. The estimates $\hat{\omega}_{\mathrm{I}}$, $\hat{\omega}_{\mathrm{II}}$, $\hat{\sigma}_{\mathrm{I}}^2$, and $\hat{\sigma}_{\mathrm{II}}^2$ are obtained as the locations and amplitudes of the two highest peaks in the AR estimated spectrum. A flag is returned if only one peak is found, as for beamforming and Capon. Note that also the continuous spectrum model of AR estimation is not perfectly matched to the data model (1)–(2), where the two spectral components have Gaussian shape.

B. Locking Methods

The aim of step 2 of the proposed procedure is to retrieve the spectral advection ω_a from the spectral parameters extracted in the MB Doppler analysis step:

$$\{\hat{\omega}_{\mathrm{I}}, \hat{\omega}_{\mathrm{II}}, \hat{\sigma}_{\mathrm{I}}^2, \hat{\sigma}_{\mathrm{II}}^2\} \rightarrow \hat{\omega}_a. \tag{10}$$

Three different techniques are proposed and investigated here for the mapping (10). They are conceived for application to three different scenarios. These correspond to different degrees of a priori information about wind direction and the value of the characteristic Bragg frequency ω_B. Starting from a condition where some information is available, the assumptions will be progressively relaxed reaching the case where no ancillary data are available.

In the first scenario, the characteristic Bragg frequency is assumed a priori known. This is reasonable for low sea state, when the local incidence angle is known from system geometry. It is also assumed to know which of the two Bragg components is dominant. This second assumption corresponds to know if the wind direction lays in the front or rear half-plane determined by the platform track, which is only a partial information about wind aspect. The locking method that we propose for this scenario is termed the most powerful peak (MPP) method. MPP aims to lock onto and compensate for the assumed dominant Bragg component, independently of the presence of a weaker component with opposite motion. The latter can arise when the actual wind aspect is not exactly upwind or downwind, in the front or rear half-plane assumption, respectively. Without loss of generality, in this work we refer to MPP designed for dominant receding Bragg waves, i.e., assuming that the wind direction lays in the rear half-plane defined by the track. First, the frequency estimates are labeled to identify the Doppler shift of the receding Bragg component, ω_2. This is obtained as

$$\hat{\omega}_2 = \begin{cases} \hat{\omega}_{\mathrm{I}} & \text{if} \quad \hat{\sigma}_{\mathrm{I}}^2 \geq \hat{\sigma}_{\mathrm{II}}^2 \\ \hat{\omega}_{\mathrm{II}} & \text{if} \quad \hat{\sigma}_{\mathrm{I}}^2 < \hat{\sigma}_{\mathrm{II}}^2 \end{cases} \tag{11}$$

or, $\hat{\omega}_2 = \hat{\omega}_{\mathrm{I}}$ when only one frequency estimate is available from step 1. Note that in both cases the information that the dominant component is the receding one is exploited. Then, locking onto the assumed dominant receding component and consequent compensation is obtained from (3) as:

$$\hat{\omega}_a = \hat{\omega}_2 + \omega_B. \tag{12}$$

In words, the MPP method for the rear half-plane assumption finds the strongest peak in the estimated spectrum, and estimates the advection ω_a as the sum of the frequency of the strongest peak and ω_B. The dual version of MPP for the front half-plane assumption can be found following a similar reasoning. The MPP is a very simple algorithm. It does not allow to obtain fully autonomous velocity estimates. Yet, it is suited to work in single as well as in dual Bragg component conditions while the wind aspect lies in a $\pm 90°$ range around downwind (or crosswind).

In the second scenario, the Bragg frequency is again assumed known, but any assumption about wind direction is relaxed. We term the technique proposed for this scenario the high dual peak (HDP) method. HDP aims to lock onto, and properly compensate for, an automatically identified dominating Bragg component, whether it is advancing or receding. Labeling of the two frequency estimates needs now a little care. Since the frequencies are measured modulo the unambiguous range, a simple algebraic ordering to identify which estimate has to be associated with the receding and the advancing component, can be misleading.[6] The circular nature of the frequency values has to be accounted for. To handle this problem we assume here, without loss of generality, that $2\omega_B$ is less than half the unambiguous range, $\pi(K-1)/\tau$. Consequently, labeling is obtained as follows:

$$[\hat{\omega}_1, \hat{\omega}_2] = \begin{cases} [\max\{\hat{\omega}_\mathrm{I}, \hat{\omega}_\mathrm{II}\}, \min\{\hat{\omega}_\mathrm{I}, \hat{\omega}_\mathrm{II}\}] \\ \qquad \text{if} \quad |\hat{\omega}_\mathrm{I} - \hat{\omega}_\mathrm{II}| < \pi(K-1)/\tau \\ [\min\{\hat{\omega}_\mathrm{I}, \hat{\omega}_\mathrm{II}\}, \max\{\hat{\omega}_\mathrm{I}, \hat{\omega}_\mathrm{II}\}] \\ \qquad \text{if} \quad |\hat{\omega}_\mathrm{I} - \hat{\omega}_\mathrm{II}| \geq \pi(K-1)/\tau. \end{cases} \tag{13}$$

$\hat{\sigma}_1^2$ and $\hat{\sigma}_2^2$ are obtained consequently. Note that both the components are exploited to automatically identify which is the advancing and which the receding component. This makes non trivial the role of this labeling stage. If one of the two Bragg components is very weak, its frequency estimate becomes erratic, or driven by the sidelobes of the spectral response from the dominating component. Consequently, labeling error can occur, and the resulting wrong association causes large "catastrophic" errors in the estimate $\hat{\omega}_a$. Also, note that when two peaks have not been found in the beamforming, Capon, or YW spectrum because of leakage (one component masked) or resolution problems, HDP cannot perform labeling and returns a "nonoperative" flag. Conversely, MPP, as well as HDP with MUSIC-LS, is always operative. After labeling, HDP locks onto the peak with the higher estimated amplitude, since frequency is more reliably estimated for the most powerful component. Compensation is carried out according to the estimated label of the dominant component, i.e., advancing of receding, as follows from (3):

$$\hat{\omega}_a = \begin{cases} \hat{\omega}_2 + \omega_B & \text{if} \quad \hat{\sigma}_2^2 \geq \hat{\sigma}_1^2 \\ \hat{\omega}_1 - \omega_B & \text{if} \quad \hat{\sigma}_2^2 < \hat{\sigma}_1^2. \end{cases} \tag{14}$$

Roughly speaking, the HDP method estimates the location of both the Bragg components by finding the two highest peaks in the estimated spectrum. Then, the two estimates are ordered modulo the unambiguous Doppler range. The strongest of the two peaks is selected, and the advection ω_a is estimated as the difference between the selected frequency and $\pm\omega_B$, where the sign depends on the advancing or receding component being selected for locking, respectively. HDP does not require any a priori knowledge on the wind direction, and aims to obtain fully autonomous velocity estimates. However, in practice it is expected that it cannot operate, or operates with large errors, in close to single Bragg component conditions. This case arises when the wind aspect is close to upwind or to downwind.

In the third scenario, it is not even assumed an exact a priori knowledge of the Bragg frequency. This makes sense, e.g., for high sea state where the local incidence angle can change around the nominal one (ϑ) because of the tilt of long waves [19]. The method conceived for this scenario is termed the averaged dual peak method (ADP). ADP has no labeling stage and exploits both peaks for locking. Under the mild assumption that $2\omega_B$ is less than half the unambiguous range, ADP estimates the advection ω_a as the mean, modulo the unambiguous Doppler range, of the frequencies of the two highest peaks. This circular mean can be obtained as

$$\hat{\omega}_a = \frac{K-1}{\tau} \arg\{\exp(j\hat{\omega}_\mathrm{I}\tau/(K-1)) + \exp(j\hat{\omega}_\mathrm{II}\tau/(K-1))\}. \tag{15}$$

ADP, as the HDP method, sometimes may be non-operative.

IV. PERFORMANCE ANALYSIS

We now numerically investigate the performance of the different estimators of ω_a using data model (1)–(3). All the spectral estimation methods that we investigated rely on an evaluation of the data covariance matrix $\mathbf{C}_y$. For beamforming and Capon methods we used a Toeplitz estimate, for the root-MUSIC method we used the forward-backward (FB) averaging approach[7] [27]. The same approach is used also for LS, replacing the sample estimate with its FB counterpart in (9), and for the YW method. Beamforming and Capon have been implemented by using the fast Fourier transform (FFT) for a first coarse search of the peak locations and the chirp zeta transform (CZT) for a local refined search.

Where not otherwise stated, all the numerical results were derived for $N = 32$ looks, total signal-to-noise ratio $\mathrm{SNR}_{Tot} = \sigma_T^2/\sigma_v^2 = 24$ dB, normalized coherence time $\tilde{\tau}_c = 4$, normalized Bragg frequency $\omega_B\tau = 3\pi/8$ rad, $K = 3$ channels. In particular, these parameters are representative of the L-band AIRSAR system [3]. In this platform, $K = 3$ equispaced phase centers are available through transmitter ping-ponging between two antennas, with overall time lag $\tau = 94$ ms [3]. The choice $K = 3$ also allows to get a flavor of achievable performance for planned spaceborne distributed MB interferometers based on a cluster of three mini-satellites [28]. In L-band AIRSAR, $\tilde{\tau}_c = 4$ corresponds to $\tau_c =$

[6]As an example, the lowest negative frequency estimate does not necessarily correspond to the receding Bragg component, if a large negative advection is present making the estimate of this component fold over becoming positive. In this condition, the negative estimate actually corresponds to the advancing component affected by the large negative shift.

[7]The Toeplitz estimate is used to keep the structure of the true covariance matrix arising from uniform sampling and signal stationarity. However, this approach is inadequate for root-MUSIC. In fact, the "Toeplitz-ized" covariance matrix estimate keeps a full rank also in the ideal case of totally correlated speckle and infinite signal-to-noise ratio, when it should have rank equal to the number of sinusoidal components [27], which in our case is two.

376 ms, which is a favorable condition arising for light wind; $\omega_B\tau = 3\pi/8$ corresponds to the Bragg propagation velocity for typical moderate off-nadir incidence angle.[8] With this choice of parameter values, the Fourier resolution limit is $\Delta\omega_{BF} = 2\pi(K-1)/(K\tau) = 4\pi/3\tau$. Thus, the distance between the Bragg components is $2\omega_B = 3\pi/4\tau < \Delta\omega_{BF}$. Without loss of generality, we set $\omega_a = 0$ (performance is circularly-invariant). Being $K = 3$, the AR model order for the YW method is set to its maximum $P = 2$. The performance of the three locking techniques coupled with beamforming, Capon, YW, and MUSIC-LS were evaluated by Monte Carlo simulation (10^4 trials). We derived bias, standard deviation (STD), and root mean square error (RMSE) of the spectral advection estimate $\hat{\omega}_a$, evaluated modulo the unambiguous range and normalized to the Bragg frequency ω_B. Note that the normalized error equals the error of estimated ocean surface velocity normalized to the Bragg propagation velocity, thus it gives straightforward indication of absolute values of velocity errors. Performance of conventional ATI ($K = 2$), for which velocity estimates are based on estimation of the Doppler centroid [5, 3], has been also evaluated for comparison. The time lag was set equal to the overall time lag of the MB system, and operating conditions are identical. Thus, N, SNR_T, $\tilde{\tau}_c$, and $\omega_B\tau$ are the same as for the MB system.

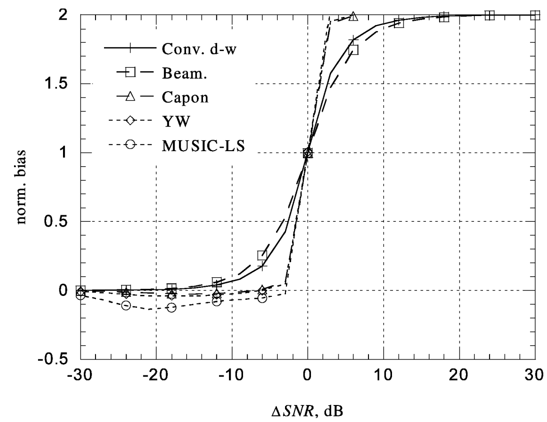

Fig. 4. Bias of estimated advection, MPP.

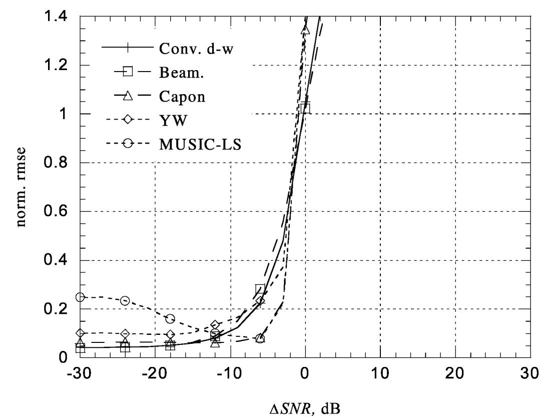

Fig. 5. RMSE of estimated advection, MPP.

A. Conventional and MPP Performance

In a first set of simulations, we investigate the effect on performance of varying power distribution between the two Bragg components: $\Delta\mathrm{SNR} = \sigma_1^2/\sigma_2^2$ is varied from -30 dB, corresponding to a practically single receding Bragg component (downwind), to 30 dB, corresponding to a single advancing Bragg component (upwind). The resulting normalized bias is reported in Fig. 4 for conventional ATI designed to operate under the downwind assumption (Conv. d-w). For increasing ΔSNR, an unexpected advancing Bragg component grows, and conventional ATI develops increasing bias. The bias limit value is twice the Bragg frequency when the advancing component is dominating. Note that for L-band AIRSAR with moderate incidence angle, this normalized bias corresponds to a velocity bias of about 120 cm/s. This is very troublesome, given that the accuracy typically required in applications is on the order of 10 cm/s [19]. Such large bias can actually occur when local wind direction is not accurately known, since the latter can be highly varying over the imaged scene [5, 21]. Conversely, MPP locking generally exhibits higher robustness while the wind direction lays in the rear half-plane relative to platform track (ΔSNR < 0 dB), at the cost of a little loss around downwind (ΔSNR = -30 dB), except MPP coupled with beamforming or MUSIC-LS. The former does not exhibit higher robustness than conventional ATI, while the latter has nonnegligible bias around downwind. When RMSE is considered, see Fig. 5, MPP-Capon performs best, and advantage over conventional ATI is obtained up to ΔSNR = -2 dB. MPP is always operative, since it can work when both a single and two Bragg components can be estimated from the data.

B. HDP Performance

Conversely from MPP, HDP locking requires that both components can be estimated. In Fig. 6, the probability of operation (P_{op}) is shown. It is defined as the probability of finding two peaks in the estimated spectrum. It gives an indication of the percentage of pixels for which the robust HDP advection estimate can be produced. HDP-beamforming is often nonoperative for ΔSNR around 0 dB (crosswind), when neither the two components can be resolved ($2\omega_B < \Delta\omega_{BF}$) nor a sidelobe appears in the estimated spectrum. Conversely, it is always operative when a single component is dominating. However, it has

[8]The assumed set of values for the normalized parameters can also represent a possible modified L-band AIRSAR system with halved overall baseline, operating at large off-nadir angle. In this case, $\tau = 47$ ms and $\tau_c = 188$ ms [18].

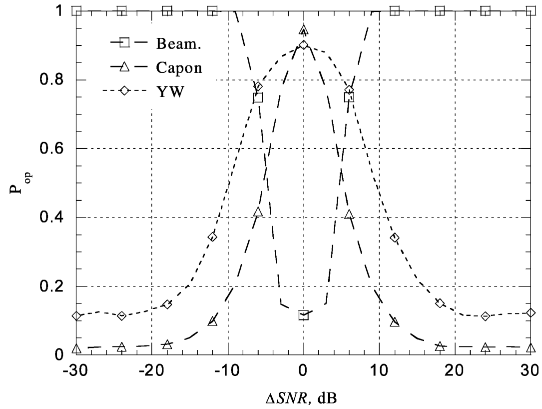

Fig. 6. Probability of operation for HDP and ADP. Probability of operation is unitary when MUSIC is employed.

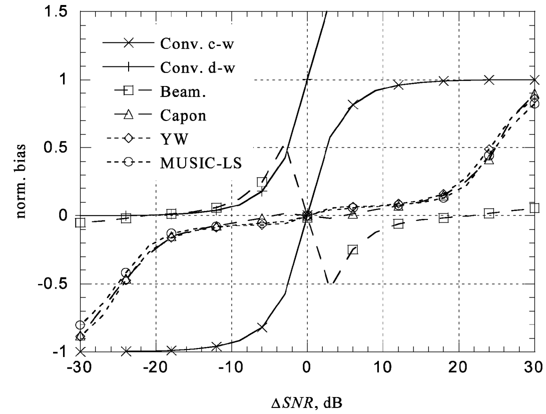

Fig. 7. Bias of estimated advection, HDP.

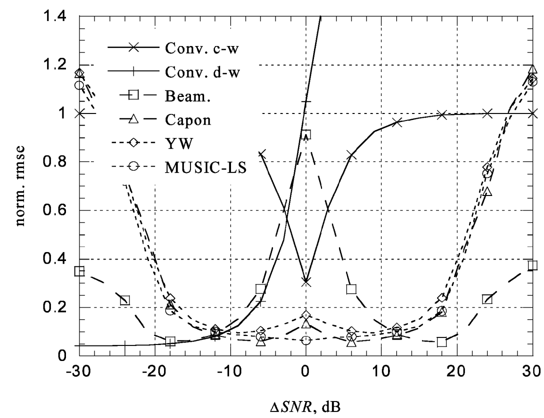

Fig. 8. RMSE of estimated advection, HDP.

to be noted that in this case one of the two peaks found is just a sidelobe, i.e., a spurious frequency estimate [24]. As expected, Capon's spectrum exhibits better resolution. HDP-Capon is often operative for ΔSNR around 0 dB, while if one component is too weak or too strong compared with the other, two peaks can be rarely found because of some leakage effect. HDP-YW generally exhibits higher P_{op} than HDP-Capon, thanks to the model-based spectral estimation producing further better resolution and reduced leakage compared with Capon. As mentioned in Section III, HDP-MUSIC-LS is always operative (P_{op} = 1).

In principle, HDP locking is conceived to work for any wind aspect, without any information about its direction. Since performance of conventional ATI for varying ΔSNR depends on the wind aspect for which it has been designed, we compare HDP performance with conventional ATI designed for operation in downwind, and for operation in crosswind. This is a significant comparison, although not exhaustive.

The normalized bias of conventional ATI operating under the crosswind assumption is shown in Fig. 7 (Conv. c-w); it equals the normalized bias of downwind-designed ATI minus one. Note the high sensitivity of conventional ATI designed for crosswind to deviations from the nominal wind aspect (ΔSNR ≠ 0 dB). The bias of HDP methods is also reported. It is apparent that a very strong bias reduction over crosswind-designed ATI is generally achieved by HDP when wind aspect deviates from the nominal direction assumed for conventional ATI. Performance of HDP-beamforming is not satisfactory around crosswind, taking also into account its low P_{op}. Interestingly, gain in terms of STD is also produced around crosswind, except by beamforming. It is worth recalling that in crosswind the total ocean coherence time is significantly lower than the coherence time τ_c of each component, for a same modulation effect from medium waves (see footnote 3). This can result in an increased STD for conventional ATI, by about 7 times compared with the single Bragg component situation, for the assumed parameters [30]. Conversely, HDP-MUSIC-LS processing can produce a STD close to that of conventional ATI operating with a single Bragg component, compensating for the loss of total coherence time around crosswind. For ΔSNR = 0 dB, STD is reduced by about 5 times compared with conventional ATI. This is because locking onto only one of the two peaks, not onto the centroid, virtually cast the problem in a single-component scenario, which is a serendipitous result. Consequently, a very good RMSE reduction compared with conventional ATI is obtained by HDP for a very large range of |ΔSNR|, as shown in Fig. 8. HDP-MUSIC-LS can be globally considered the best performing method, taking account also of its unitary P_{op}. When HDP performance is compared with conventional ATI designed for the downwind assumption, strong bias reduction is again observed. Bias of 18% at ΔSNR = −6 dB is reduced to −5.5% by HDP-MUSIC-LS, and bias of 100% at ΔSNR = 0 dB is canceled. However, a loss in terms of bias results for ΔSNR < −10 dB, see Fig. 7. This is because HDP needs two significant components being present to correctly identify the right one for locking. Consequently, large gain in

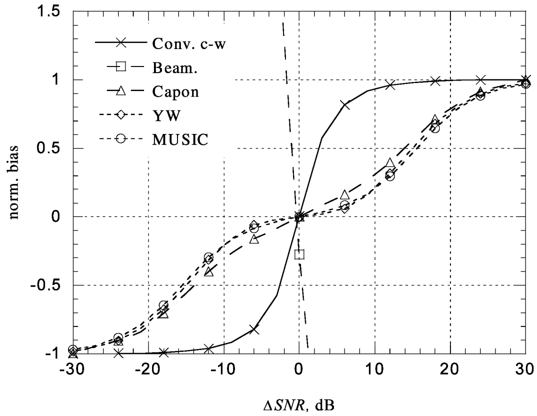

Fig. 9. Bias of estimated advection, ADP.

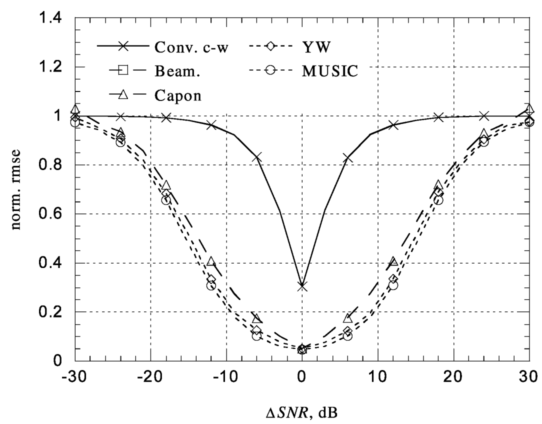

Fig. 10. RMSE of estimated advection, ADP.

terms of RMSE is now obtained for all wind aspects except for close to downwind, where the "matched" conventional ATI is better;[9] see Fig. 8.

C. ADP Performance

Bias and RMSE of ADP locking, which can operate with unknown ω_B, is reported in Figs. 9 and 10, and compared with conventional ATI designed for crosswind. The probability of operation P_{op} for ADP is the same as for HDP (Fig. 6). Interestingly, bias control capability around crosswind is still good despite the lack of information of Bragg frequency ω_B, although some degradation compared with HDP can be noted for large $|\Delta\mathrm{SNR}|$. Conversely, a slight RMSE accuracy gain over HDP is even obtained for $\Delta\mathrm{SNR} \approx 0$ dB, thanks to the averaging effect coming from exploiting both peaks for locking. However, RMSE gain over crosswind-designed conventional ATI is reduced for large deviations from crosswind. ADP-MUSIC is the best performing method. The

[9]It is worth noting that the catastrophic errors from wrong labeling are impulsive. Thus, they may be significantly reduced by spatial median filtering of the estimated velocity map.

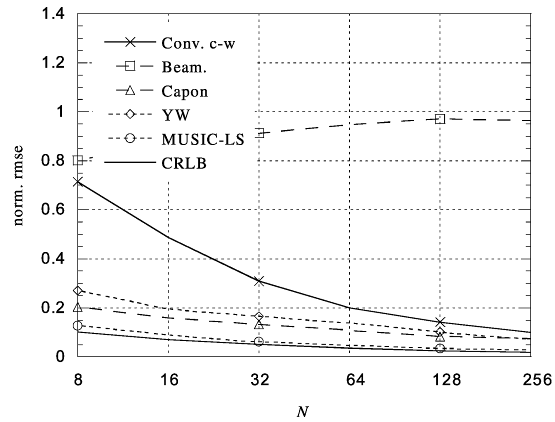

Fig. 11. RMSE of estimated advection, HDP, $\Delta\mathrm{SNR} = 0$ dB.

other ADP methods have close performance, except ADP-beamforming, whose RMSE is out of scale.

D. Analysis of Statistical Efficiency, Threshold Effect, and Bragg Component Resolution

In a second set of simulations, we focus on HDP locking, which is particularly effective in overcoming the troublesome sensitivity of conventional ATI designed for crosswind. We investigate its performance in terms of asymptotic efficiency, threshold effect, robustness to multiplicative noise, and resolution problems. The CRLB on the advection estimate $\hat{\omega}_a$ has been also evaluated, assuming that ω_B is known. The derivation is reported in the Appendix. This CRLB is the extension of the classical interferometric CRLB in [31] to the case of MB data and dual Bragg component condition. It is used in the sequel to judge the statistical efficiency of HDP estimators, and may be also exploited for analytical performance prediction and system optimization. In the following, $\Delta\mathrm{SNR}$ is set to 0 dB (crosswind) and the other parameters are set as above. Performance is also compared with crosswind-designed conventional ATI.

The influence of the number of looks is shown in Fig. 11. For varying N, bias of all the methods is almost unaltered [30], while STD decreases with increasing N, as expected. RMSE ranking among the methods does not change with N for the given parameter set. HDP-MUSIC-LS is the most statistically efficient method; it is also quite close to the CRLB. However, it seems that it does not asymptotically achieve the bound (for $N = 256$ its RMSE is still 1.5 times the CRLB). This may be attributed to the fact that MUSIC operates under model mismatch and only a single component is used for locking, thus part of the data information content is not exploited. The influence of critical signal power levels, possible for smooth ocean or far range [3], is investigated in Fig. 12. The result is that HDP can

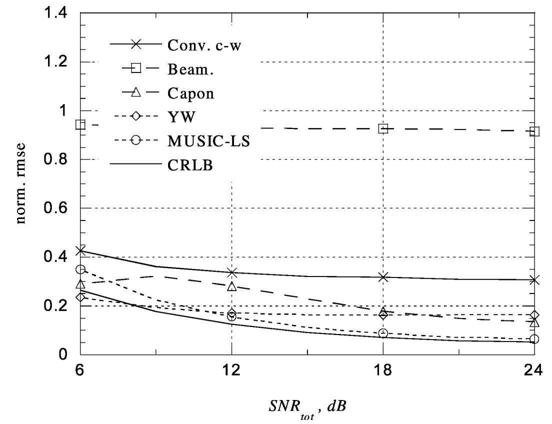

Fig. 12. RMSE of estimated advection, HDP, ΔSNR = 0 dB.

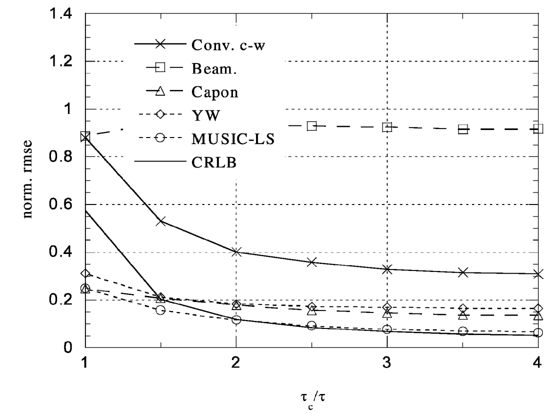

Fig. 13. RMSE of estimated advection, HDP, ΔSNR = 0 dB.

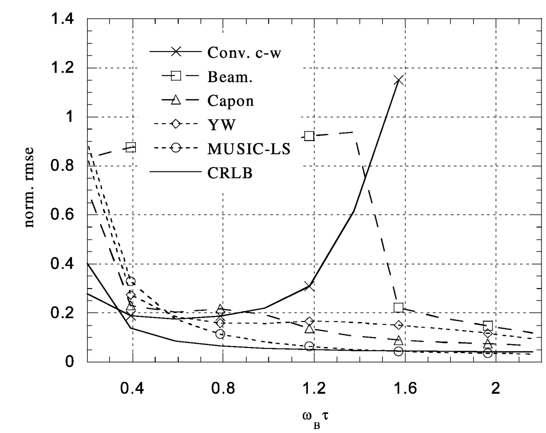

Fig. 14. RMSE of estimated advection, HDP, ΔSNR = 0 dB.

perform well also for low $\mathrm{SNR}_{\mathrm{tot}}$, still producing a gain over conventional ATI. HDP-MUSIC-LS is quite efficient for large $\mathrm{SNR}_{\mathrm{tot}}$, while HDP-YW exhibits a lower threshold effect, at the cost of the nonunitary P_{op}. For $\mathrm{SNR}_{\mathrm{tot}} < 8$ dB, it gets an RMSE lower than that of any unbiased estimator, trading off bias for variance [32]. HDP can perform well also under critical coherence conditions, as shown in Fig. 13. Notably, for decreasing τ_c, i.e., increasing bandwidth of the speckle processes, the continuous AR spectrum model of YW does not produce appreciable benefits compared with the discrete spectrum model of MUSIC-LS. HDP-MUSIC-LS is still the most efficient among the HDP methods, followed by HDP-Capon. However, keeping good performance at low τ_c is increasingly difficult for large deviations from crosswind ($\Delta\mathrm{SNR} \neq 0$ dB), for the assumed N and $\mathrm{SNR}_{\mathrm{tot}}$ [30]. The RMSE as a function of the normalized frequency $\omega_B\tau$ is reported in Fig. 14. For decreasing frequency separation between the two Bragg components the gain of HDP tends to decrease, because of the increasingly challenging resolution problem. In particular, when operation in C-band is considered [3], $\omega_B\tau$ is typically in the range [0.3, 0.4] rad, i.e., around 1/4 to 1/3 of the corresponding value for L-band, while τ_c/τ can be considered the same, being both the typical overall time lag and coherence time lower than for L-band [3, 5]. It is worth noting that the inversion problem affecting conventional ATI is troublesome also at C-band, where velocity bias up to about 60 cm/s is possible. Unfortunately, in this condition the gain of HDP over crosswind-designed conventional ATI vanishes. However, room for future performance improvement is shown by the CRLB at $\omega_B\tau =$ 0.4, corresponding to C-band AIRSAR operating with large off-nadir angle. Moreover, gain over "mismatched" downwind-designed conventional ATI, whose normalized RMSE is 1.02, is still produced. HDP-Capon now exhibits the lowest RMSE, at the cost of a very low $P_{\mathrm{op}} = 0.1$, followed by HDP-YW ($P_{\mathrm{op}} = 0.3$) and HDP-MUSIC-LS which trades off accuracy for operational capability.

Despite focus in this work is on curing the effects of lack of detailed wind direction information, it is now worth stressing another potential of the robust velocity estimators. Even when wind information is available, it is not always possible to accurately predict the Bragg power split ratio, because the hydrodynamic modulation effect by current gradients can change the relative intensity of the advancing and receding Bragg waves compared with stationary current areas [5]. As a result, the conventional ATI current imaging can be locally nonlinear (especially at L-band) [19, p. 453], since the relationship between measured Doppler centroid and desired current estimate can change with the current itself. In this framework, MB acquisition and processing robust to unknown Bragg power split ratio may be useful also to get more linear ATI current imaging. This potential is not investigated further here and is left as matter for future research. It is also worth recalling how one can postprocess the advection (velocity) estimates to decouple the actual current velocity from the total (orbital + current) velocity measured in the ATI framework, in which long waves are treated deterministically. Decoupling is based on the fact that the orbital velocity field is zero-mean, thus local spatial (incoherent) averaging of the total estimated velocity over a number of wave periods results in the current velocity only [20].[10]

V. CONCLUSIONS

In this work we considered the problem of estimating ocean surface velocity when only partial or no information from ancillary data is available to compensate for the net Bragg velocity. A first step has been taken towards making ATI sensing flexible and possibly autonomous from wind information by exploiting baseline diversity. Three classes of robust MB surface velocity estimation techniques have been presented to operate under different degrees of availability of a priori information on wind direction and Bragg frequency. Estimation accuracy has been analyzed by simulation and CRLB calculation. Interestingly, two baselines can be enough to get velocity estimates that are not sensibly hampered by the uncertain bimodal Doppler spectrum. None of the estimators in each class is uniformly the most efficient. Compared with conventional ATI, good performance is provided by MPP-Capon, which exhibits robustness to deviations from an upwind or downwind assumption. HDP-MUSIC-LS generally produces much better performance than conventional ATI for a wide range of wind aspects around crosswind. ADP-MUSIC can operate satisfactorily even with unknown Bragg frequency.

The performance analysis reported is valid for L- and C-band systems and light to gentle wind. The effective limits of validity of the analysis for stronger wind speed are the subject of future research work. Validation with real airborne data is in order. The results obtained can be used to develop a hybrid technique adaptively selecting algorithms in the same class, as well as integrating the HDP class with MPP to further extend the range of wind aspects for which good operation is obtained. System optimization of the overall time lag for MB processing can be also analyzed, some indications can be found in [18]. Both airborne and future spaceborne ATI systems [28] may benefit from the proposed MB technique. It can be employed alternatively to or jointly with carrier and off-nadir angle optimization to minimize ATI sensitivity to uncertainty of bimodal spectrum [19], obtaining a better overall system design in presence of contrasting requirements. Moreover, synergy with vector-ATI concepts [13] and multifrequency ATI [21] can be considered.

[10]When the orbital velocity is not exactly zero-mean because of the so-called Stokes drift (small net velocity in the wave direction), the non-zero mean enters the current velocity obtained by postprocessing. This is actually good from the measurement perspective, since the Stokes drift can be considered as one of the components of the surface current [20], besides those from wind drift, tides, etc.

APPENDIX. CRLB FOR MB ADVECTION ESTIMATION

In the following, we derive the CRLB on the estimation of ω_a for the MB ATI signal model in (1)–(3). Denote with $\boldsymbol{\chi} = [\sigma_1^2,\ \sigma_2^2,\ \sigma_v^2,\ \tau_c/\tau,\ \omega_a\tau]^T$ the vector of all the unknown parameters. The normalized Bragg frequency $\omega_B\tau$ is assumed here to be known. The elements of the Fisher information matrix (FIM) for the zero-mean complex Gaussian distributed data vector in (1) are [26]

$$[\mathbf{J}_{\mathrm{FIM}}]_{i,j} = \mathrm{tr}\left\{\mathbf{C}_y^{-1}\frac{\partial \mathbf{C}_y}{\partial \chi_i}\mathbf{C}_y^{-1}\frac{\partial \mathbf{C}_y}{\partial \chi_j}\right\} \tag{16}$$

where $\mathrm{tr}\{\cdot\}$ is the trace operator, and $\chi_i = [\boldsymbol{\chi}]_i$. From (1) the data covariance matrix is

$$\mathbf{C}_y = \sum_{m=1}^{2}\sigma_m^2\mathbf{A}(\omega_m\tau)\mathbf{C}_x\mathbf{A}^H(\omega_m\tau) + \sigma_v^2\mathbf{I} \tag{17}$$

with $\mathbf{C}_x$ given by (2), $\omega_1\tau = \omega_a\tau + \omega_B\tau$, and $\omega_2\tau = \omega_a\tau - \omega_B\tau$. The partial derivatives of (17) are

$$\begin{aligned}
&\frac{\partial \mathbf{C}_y}{\partial \sigma_m^2} = \mathbf{A}_m\mathbf{C}_x\mathbf{A}_m^H, \qquad \frac{\partial \mathbf{C}_y}{\partial \sigma_v^2} = \mathbf{I}\\
&\frac{\partial \mathbf{C}_y}{\partial(\tau_c/\tau)} = \left[\sum_{m=1}^{2}\sigma_m^2\mathbf{A}_m\mathbf{C}_x\mathbf{A}_m^H\right]\odot\mathbf{L}_T\\
&\frac{\partial \mathbf{C}_y}{\partial(\omega_a\tau)} = j\left[\sum_{m=1}^{2}\sigma_m^2\mathbf{A}_m\mathbf{C}_x\mathbf{A}_m^H\right]\odot\mathbf{L}_A
\end{aligned} \tag{18}$$

where $\odot$ denotes the Hadamard product [27], and $\mathbf{A}_m = \mathbf{A}(\omega_m\tau)$. $\mathbf{L}_T$ and $\mathbf{L}_A$ are two $K\times K$ Toeplitz matrices having elements:

$$[\mathbf{L}_T]_{i,j} = -2\frac{(i-j)^2}{(K-1)^2}\tau_c/\tau, \qquad [\mathbf{L}_A]_{i,j} = \frac{i-j}{K-1}, \qquad 1\le(i,j)\le K. \tag{19}$$

The bound on $\hat{\omega}_a\tau$ is easily evaluated numerically as $N^{-1}[\mathbf{J}_{\mathrm{FIM}}^{-1}]_{5,5}$ [26], where $\mathbf{J}_{\mathrm{FIM}}$ is the FIM for a single look which is readily obtained by plugging (17), (18) and (19) in (16). In Figs. 11–14 $\sqrt{\mathrm{CRLB}(\hat{\omega}_a)}/\omega_B$ is reported, which is obtained as $\sqrt{\mathrm{CRLB}(\hat{\omega}_a\tau)}/\omega_B\tau$.

REFERENCES

[1] Goldstein, R. M., and Zebker, H. A. (1987)
Interferometric radar measurement of ocean surface currents.
Nature, **328**, 20 (Aug. 1987), 707–709.

[2] http://airsar.jpl.nasa.gov/documents/workshop2002/papers/O1-O11.pdf

[3] Carande, R. E. (1994)
Estimating ocean coherence time using dual-baseline interferometric synthetic aperture radar.
IEEE Transactions on Geoscience and Remote Sensing, **32**, 4 (July 1994), 846–854.

[4] Imel, D. A. (2002)
AIRSAR along-track interferometry data.
In *Proceedings of the 2002 AIRSAR Earth Science and Application Workshop*, Pasadena, CA.
http://airsar.jpl.nasa.gov/documents/workshop2002/papers/O1.pdf

[5] Thompson, D. R., and Jensen, J. R. (1993)
Synthetic aperture radar interferometry applied to ship-generated internal waves in the 1989 Loch Linnhe experiment.
Journal of Geophysical Research, **C6** (June 1993), 10259–10269.

[6] Ainsworth, T. L., Chubb, S. R., Fusina, R. A., Goldstein, R. M., Jansen, R. W., Lee, J-S., and Valenzuela, G. R. (1995)
INSAR imagery of surface currents, wave fields, and fronts.
IEEE Transactions on Geoscience and Remote Sensing, **33**, 5 (Sept. 1995), 1117–1123.

[7] Hasselmann, K., Raney, R. K., Plant, W. J., Alpers, W., Shuchman, R. A., Lyzenga, D. R., Rufenach, C. L., and Tucker, M. J. (1985)
Theory of synthetic aperture radar ocean imaging: A MARSEN view.
Journal of Geophysical Research, **90** (1985), 4659–4686.

[8] Henderson, F., and Lewis, A. (1998)
Principles and applications of imaging radar.
In *Manual of Remote Sensing, Vol. 2*, New York: Wiley, 1998.

[9] Shemer, L. et al. (1993)
Estimates of currents in nearshore ocean region using interferometric synthetic aperture radar.
Journal of Geophysical Research, **C4** (1993), 7001–7010.

[10] Lyzenga, D., and Malinas, N. (1996)
Azimuth falloff effects in two-antenna SAR measurements of ocean wave spectra.
IEEE Transactions on Geoscience and Remote Sensing, **34**, 4 (July 1996), 1020–1028.

[11] Bao, M., Bruning, C., and Alpers, W. (1997)
Simulation of ocean waves imaging by along-track interferometric synthetic aperture radar.
IEEE Transactions on Geoscience and Remote Sensing, **35**, 3 (May 1997), 618–631.

[12] Frasier, S. J., and Camps, A. J. (2001)
Dual-beam interferometry for ocean surface current vector mapping.
IEEE Transactions on Geoscience and Remote Sensing, **39**, 2 (Feb. 2001), 401–414.

[13] Moller, D., Pollard, B., and Rodriguez, E. (2002)
Feasibility study and system design for a spaceborne along-track interferometer/scatterometer.
In *Proceedings of 2002 AIRSAR Earth Science and Application Workshop*, Pasadena, CA.
http://airsar.jpl.nasa.gov/documents/workshop2002/papers/O5.pdf

[14] Rosen, P. A., Hensley, S., Joughin, I. R., Li, F. K., Madsen, S. N., Rodriguez, E., and Goldstein, R. M. (2000)
Synthetic aperture radar interferometry.
Proceedings of the IEEE, **88**, 3 (Mar. 2000), 333–382.

[15] Friedlander, B., and Porat, B. (1998)
VSAR: A high-resolution radar system for ocean imaging.
IEEE Transactions on Aerospace and Electronic Systems, **34**, 3 (July 1998), 755–776.

[16] Besson, O., Gini, F., Griffiths, H. D., and Lombardini, F. (2000)
Estimating ocean surface velocity and coherence time using multichannel ATI-SAR systems.
IEE Proceedings, Pt. F, **147**, 6 (Dec. 2000), 299–308.

[17] Barber, B. (2000)
Recent advances in ocean remote sensing using imaging radar.
Journal of Defence Science, **5**, 3 (2000), F50–F58.

[18] Lombardini, F., Bordoni, F., and Gini, F. (2002)
Enhanced and new possible functionalities of ATI-SAR through multibaseline acquisition and modern spectral estimation techniques.
In *Proceedings of 2002 AIRSAR Earth Science and Application Workshop*, Pasadena, CA.
http://airsar.jpl.nasa.gov/documents/workshop2002/papers/O9.pdf

[19] Romeiser, R., and Thompson, D. R. (2000)
Numerical study on the along-track interferometric radar imaging mechanism of oceanic surface currents.
IEEE Transactions on Geoscience and Remote Sensing, **38**, 1 (Jan. 2000), 446–458.

[20] Moller, D., Frasier, S. J., Porter, D. L., and McIntosh, R. E. (1998)
Radar-derived interferometric surface currents and their relationship to subsurface current structure.
Journal of Geophysical Research, **103**, C6 (June 1998), 12,839–12,852.

[21] Kim, D., Moon, W. M., Imel, D. A., and Moller, D. (2002)
Remote sensing of ocean waves and currents using AIRSAR along-track interferometry (ATI).
In *Proceedings of 2002 AIRSAR Earth Science and Application Workshop*, Pasadena, CA.
http://airsar.jpl.nasa.gov/documents/workshop2002/papers/O2.pdf

[22] Orwig, L., and Held, D. (1992)
Interferometric ocean surface mapping and moving object relocation with a Norden Systems Ku-band SAR.
In *Proceedings of IEEE 1992 International Geoscience and Remote Sensing Symposium*, Houston, TX, May 1992, 1598–1600.

[23] Ender, J. H. G. (1997)
Space-time adaptive processing for synthetic aperture radar.
In *IEE Colloquium on Space-Time Adaptive Processing*, Savoy Place, London, Apr. 1997, 4/1-4/6.

[24] Lombardini, F., Gini, F., and Matteucci, P. (2001)
Multibaseline ATI-SAR for robust ocean surface velocity estimation in presence of bimodal Doppler spectrum.
In *Proceedings of IEEE 2001 International Geoscience and Remote Sensing Symposium*, Sydney, Australia.

[25] Chapman, R. D., Gotwols, B. L., and Sterner II, R. E. (1994)
On the statistics of the phase of microwave backscatter from the ocean surface.
Journal of Geophysical Research, **99**, C8 (Aug. 1994), 16,293–16,301.

[26] Kay, S. M. (1993)
Fundamentals of Statistical Signal Processing, Estimation Theory.
Englewood Cliffs, NJ: Prentice-Hall, 1993.

[27] Stoica, P., and Moses, R. (1997)
Introduction to Spectral Analysis.
Englewood Cliffs, NJ: Prentice-Hall, 1997.

[28] Fiedler, H., Krieger, G., Jochim, F., Kirschner, M., and Moreira, A. (2002)
Analysis of bistatic configurations for spaceborne SAR interferometry.
In *Proceedings of the 4th European Conference on Synthetic Aperture Radar*, Cologne, Germany, June 2002, 29–32.

[29] Lombardini, F., Gini, F., and Matteucci, P. (2001)
Application of array processing techniques to multibaseline InSAR for layover solution.
In *Proceedings of the 2001 IEEE Radar Conference*, May 2001, Atlanta, GA.

[30] Bordoni, F., Gini, F., Lombardini, F., and Verrazzani, L. (2002)
Algorithms for robust multibaseline ATI-SAR ocean surface velocity estimation in the presence of bimodal Doppler spectrum.
Technical report, Editrice Tecnico Scientifica, Pisa, Italy, May 2002.

[31] Rodriguez, E., and Martin, J. M. (1992)
Theory and design of interferometric synthetic aperture radars.
IEE Proceedings, Pt. F, **139**, 2 (Apr. 1992), 147–159.

[32] Gini, F. (1996)
Estimation strategies in the presence of nuisance parameters.
Signal Processing, **55**, 2 (1996), 241–245.

Fabrizio Lombardini (M'93—SM'03) received the Italian Laurea degree, with honors, in electronic engineering and the Ph.D. degree in telecommunication engineering from the University of Pisa, Italy, in 1993 and 1997, respectively.

He was granted by the EU a Marie Curie Fellowship of the Training and Mobility of Researchers (TMR) Program, which he spent as postdoctoral researcher at the Department of Electronic and Electrical Engineering of University College London, U.K., from 1998 to 1999. Then, he joined the Department of "Ingegneria della Informazione" of University of Pisa, where he currently holds the permanent position of assistant professor. He is IEEE member since 1993 and senior member since January 2003. He has given lectures at universities and institutions in Italy and abroad, and has organized sessions at international conferences.

His general interests are in the areas of statistical signal processing, estimation and detection theory, adaptive and super-resolution spectral analysis, array processing, and performance bounds evaluation, with application to radar systems. In particular, his research interests include multibaseline and multifrequency interferometric SAR algorithms and systems, both cross- and along-track, multibaseline SAR tomography, multisensor data fusion, and radar detection in non-Gaussian clutter.

F. Bordoni received the Doctor Engineer degree in telecommunication engineering from the University of Pisa, Italy, in 2001. She is currently pursuing the Ph.D. degree in telecommunication engineering from the University of Pisa, where she is working with the Signal Processing and Remote Sensing Group.

Her general interests are in the areas of statistical signal processing, estimation and detection theory and statistical analysis of radar clutter data. In particular, her research interests include modern spectral estimation and detection techniques for multichannel signal processing, with application both in the field of SAR interferometry and radar processing.

Fulvio Gini (S'93—M'95—SM'00) received the Doctor Engineer (cum laude) and the Research Doctor degrees in electronic engineering from the University of Pisa, Italy, in 1990 and 1995 respectively.

In 1993 he joined the Department of "Ingegneria dell'Informazione" of the University of Pisa, where he is an associate professor since October 2000. From July 1996 through January 1997, he was a visiting researcher at the Department of Electrical Engineering, University of Virginia, Charlottesville. He has been session chairman at international conferences. He is coauthor of two tutorials entitled "Coherent detection and fusion in high resolution radar systems" presented at the International Conference on Radar (May 1999, Brest) and "Advanced Radar Detection and Fusion" presented at the International Radar Conference (May 2000, Washington D.C.). In February 2002 he was the faculty opponent at the Chalmers University of Technology, for a Ph.D. thesis defense. He is IEEE member since 1992 and senior member since January 1, 2000. He is an associate editor for the IEEE Transactions on Signal Processing (term starting August 1, 2000) and a member of the EURASIP JASP Editorial Board (term starting July 1, 2003). He was corecipient of the 2001 IEEE Aerospace and Electronic Systems Society's Barry Carlton Award for Best Paper. He was recipient of the 2003 IEE Achievement Award for outstanding contribution in signal processing and of the 2003 IEEE Aerospace and Electronic Systems Society Nathanson Award to the Young Engineer of the Year. He is a member of the Signal Processing Theory and Methods (SPTM) Technical Committee (TC) of the IEEE Signal Processing Society since January 1, 2003.

His general interests are in the areas of statistical signal processing, estimation and detection theory. In particular, his research interests include modeling and statistical analysis of recorded live sea and ground radar clutter data, non-Gaussian signal detection and estimation, parameter estimation and data extraction from multichannel interferometric SAR data, cyclostationary signal analysis, and estimation of nonstationary signals, with applications to radar signal processing. He authored or coauthored more than 60 journal papers and about 60 conference papers.

Lucio Verrazzani received the Dr. Ing. degree (cum laude) in electrical engineering from the University of Pisa, Italy, in 1962 and the "Libera Docenza" in applied electronics from the same university in 1972.

Since 1962 he has been working at the Institute of Electronics and Telecommunications. He is currently a full professor of signal theory at the Engineering Faculty of Pisa, Italy, and invited professor at Accademia Navale of the Italian Navy in Livorno. He is engaged in research on communication systems design, signal processing with application to radar and data transmission, radar target classification and identification.

His research interests include non-Gaussian clutter models, deconvolution methods relying on polispectral analysis, and data fusion in multisensor systems.